Letter to the Editor

T_2 relaxation time elongation of hepatocellular carcinoma relative to native liver tissue leads to an underestimation of perfusion fraction measured by standard intravoxel incoherent motion magnetic resonance imaging

Fu-Zhao Ma, Yì Xiáng J. Wáng

Department of Imaging and Interventional Radiology, Faculty of Medicine, The Chinese University of Hong Kong, Shatin, New Territories, Hong Kong SAR, China

Correspondence to: Yì Xiáng J. Wáng, PhD. Department of Imaging and Interventional Radiology, Faculty of Medicine, The Chinese University of Hong Kong, 30-32 Ngan Shing Street, Shatin, New Territories, Hong Kong SAR, China. Email: yixiang_wang@cuhk.edu.hk.

Submitted Oct 13, 2023. Accepted for publication Nov 14, 2023. Published online Nov 29, 2023.
doi: 10.21037/qims-23-1437
View this article at: https://dx.doi.org/10.21037/qims-23-1437

Hepatocellular carcinomas (HCCs) mostly show higher perfusion compared with adjacent normal liver tissue, reflecting their hypervascular nature (1,2). With computed tomography (CT) perfusion, Sahani *et al.* (3) measured blood flow (mL/100 g/min), blood volume (mL/100 g), and mean transit time (second) to be 92.8±88.6, 4.9±3.5, and 8.1±3.1 for HCC, whereas 14.9±2.8, 2.6±0.9, and 14.9±2.3 for background liver (with or without liver cirrhosis). With perfusion magnetic resonance imaging (MRI), Abdullah *et al.* (4) reported normalized total perfusion (mL/100 g/min) of HCC to corresponding tumor free liver to be 4.0 (range, 0.5–16.5). With perfusion MRI, Pahwa *et al.* (5) reported contrast distribution value was 49.0%±20.5% for HCC and 29.4%±8.3% for liver tissue. With perfusion CT, Ippolito *et al.* (6) reported median tissue blood volume (mL/100 g) was 20.4 for HCC and 10.9 for cirrhotic liver parenchyma. Using diffusion derived vessel density (DDVD) parameter (7,8) measuring the diffusion-weighted imaging (DWI) signal difference between b=0 and b=2 s/mm^2 data of 72 HCC patients, we found HCC had a higher DDVD measure than the background liver, with the median ratio of HCC DDVD to background liver DDVD being around 3.0 (authors' unpublished results).

Intravoxel incoherent motion (IVIM) theory in MRI was proposed by Le Bihan *et al.* to account for the effect of vessel/capillary perfusion on the aggregate magnetic resonance (MR) DWI signal. The fast component of diffusion is related to micro-perfusion, whereas the slow component is linked to molecular diffusion. Three parameters can be computed. Dslow (D_s, or D) is the diffusion coefficient representing the slow molecular diffusion (unaffected by perfusion). The perfusion fraction (*PF*, or *f*) represents the fraction of the compartment related to (micro)circulation, which can be understood as the proportional 'incoherently flowing fluid' (i.e., blood) volume. Dfast (D_f, or D^*) is the perfusion-related diffusion coefficient representing speed. IVIM has been applied to evaluate perfusion component of HCC. Paradoxically, most authors, such as Penner *et al.* (9), Zhu *et al.* (10), Woo *et al.* (11), Shan *et al.* (12), and Hectors *et al.* (13), reported a decreased *PF* of HCC relative to adjacent liver. In the meantime, with perfusion MRI, Hectors *et al.* (13) also reported a higher total blood flow of HCC than the adjacent liver.

In this letter, we propose that *PFm* (measured *PF* with IVIM imaging) is underestimated in the cases of HCC and this underestimation phenomenon is at least partially caused by the HCC's T_2 relaxation time (T_2) elongation relative to adjacent liver tissue. If the tissue diffusion component and the tissue perfusion component have separate T_2 relaxation times of T_{2t} (T_2 of the tissue diffusion component) and T_{2p} (T_2 of the perfusion component, i.e., blood) respectively, to count for T_2 dependency the standard IVIM model can be modified as [see Jerome *et al.* (14) and Lemke *et al.* (15)]:

$$S(b,TE)=S_0\left((1-PF)\cdot e^{-TE/T_{2t}}e^{-bD_s}+PF\cdot e^{-TE/T_{2p}}e^{-bD_f}\right) \quad [1]$$

where S_0 is a scaling term independent of both diffusion and 'T_2 effect' (which is defined as MRI signal differences contributed by T_2 difference), and it is implicitly assumed that repetition time is long enough to ensure no significant modulation of the signal from incomplete *T1* relaxation. Considering T_2 does not have a linear relationship with DWI signal intensity and T_2 effect cannot be eliminated by normalizing with the signal intensity at *b*=0, we can divide Eq. [1] by $(1-PF)e^{-TE/T_{2t}}+(PF)e^{-TE/T_{2p}}$, and Eq. [1] can also be written as [see Jerome *et al.* (14)]:

$$\begin{aligned}S(b,TE)=S_0&\left((1-PF)\cdot e^{-TE/T_{2t}}+PF\cdot e^{-TE/T_{2p}}\right)\\&\cdot\left((1-PFm)e^{-bD_s}+PFm\,e^{-bD_f}\right)\end{aligned} \quad [2]$$

Where *PFm* is the DWI measured PF which can be obtained by fitting the signal intensity of different *b*-values:

$$PFm(TE)=\frac{PF\cdot e^{-TE/T_{2p}}}{(1-PF)\cdot e^{-TE/T_{2t}}+PF\cdot e^{-TE/T_{2p}}} \quad [3]$$

Thus, *PFm* is *PF* taking into consideration its T_2 dependency as shown with Eq. [3], and which is a parameter we actually measure. Eq. [3] can be simplified as:

$$PFm(TE)=\frac{1}{\eta\cdot e^{-\alpha\cdot TE}+1} \quad [4]$$

Where $\eta=\frac{1-PF}{PF}$, $\alpha=\frac{1}{T_{2t}}-\frac{1}{T_{2p}}$.

Parameters *PFm*, T_{2t} and T_{2p} can be obtained by DWI data points with various time of echo (TE) and *b*-values by Eq. [4].

When *b*-value is sufficiently large, the perfusion component will decay to be minimal, and the signal intensity will be:

$$S(b,TE)=S_0\cdot(1-PF)\cdot e^{-TE/T_{2t}}e^{-bD_s} \quad [5]$$

If we take logarithm, then:

$$Log\left[S(b,TE)\right]=-\frac{TE}{T_{2t}}+\log\left(S_0\cdot(1-PF)e^{-bD_s}\right) \quad [6]$$

For the data points with same *b* value and various TE, logarithm of signal intensity is linear to the TE and the slope will be $1/T_{2t}$. Using data with identical *b*-value and various TEs, the value of T_{2t} can be directly fitted by the least square method. After obtaining the specific value of η and T_{2t}, we then know the result of T_{2p}.

For the standard DWI sequence with given TE, *PFm* can be regarded as a function of T_{2t},T_{2p} and actual *PF* as below:

$$PFm\left(PF,T_{2t},T_{2p}\right)=\frac{1}{\frac{1-PF}{PF}\cdot e^{-\frac{TE}{T_{2t}}}\cdot e^{\frac{TE}{T_{2p}}}+1} \quad [7]$$

With the methods discussed above and assuming TE could be very short (i.e., close to zero) so to eliminate the T_2 effect, Jerome *et al.* (14) estimated liver *PF* (*PFm* when TE =0) to be 0.08 (*Figure 1*). This would suggest that *PF* in normal liver is routinely overestimated with the standard IVIM assessment when TE of around 60 ms is commonly applied. In experimental physiology studies, it was suggested that the hepatic blood volume including that of the large vessels is about 25 mL/100 g (16,17). That *PF* of 0.08 is notably lower than the results obtained by other methods also suggests that *PF* may not be straightforwardly interpreted as a physiological perfusion volume fraction. We commonly estimated healthy liver *PFm* to be 0.18 (excluding large vessels) (18,19) when a TE of around 60 ms was applied. Note that *PFm* calculated with bi-exponential IVIM model is assumed to reflect fast diffusion contributed by both arteries and veins (13,20). In the study of Jerome *et al.* (14), the estimation of T_{2t} and T_{2p} of healthy liver at 1.5 Tesla (T) was around 38 ms (*Figure 2*) and around 80 ms respectively. T_{2t} is close to the T_{2a} (T_{2a} refers to the measured T_2 contributed by both T_{2t} and T_{2p}) of liver reported by other authors (21-23) while T_{2p} is notably different to the literature value (24-26). Two possibilities may explain why the measurement of T_{2p} was less stable. In the study of Jerome *et al.*, T_{2t} and α were estimated initially with two separate least square fittings, and T_{2p} was calculated later. The bias of each fitting would have accumulated for the calculation of T_{2p}. Moreover, $1/T_{2p}$ was obtained prior to its reciprocal. Given that T_{2p} is around 100 ms, slight disturbance at fitting would influence the value of $1/T_{2p}$ substantially.

In this letter, the liver's T_{2p} as 80 ms from the model estimation of Jerome *et al.* (14) and 180 ms of measured results in literature (24-26) are tested for the analysis of HCC *PFm* dependency of its T_{2a} value. We demonstrate the *PFm* dependence of T_{2p} and T_{2t} with actual *PF* =0.08 and TE =55 ms. A number of authors reported that the T_{2a} of HCC is around 60 ms with adjacent liver tissue's T_{2a} being around 40 ms (27-29). If HCC occurred at the background of liver fibrosis, the differences between liver fibrotic tissue and HCC are assumed already considered (27-29). Higher HCC T_{2a} have also been reported (HCC and metastasis have approximately similar T_{2a}) (30,31), which could be related to the differentiation of the HCC. Poorly differentiated HCCs may have deviated more from native liver tissue with

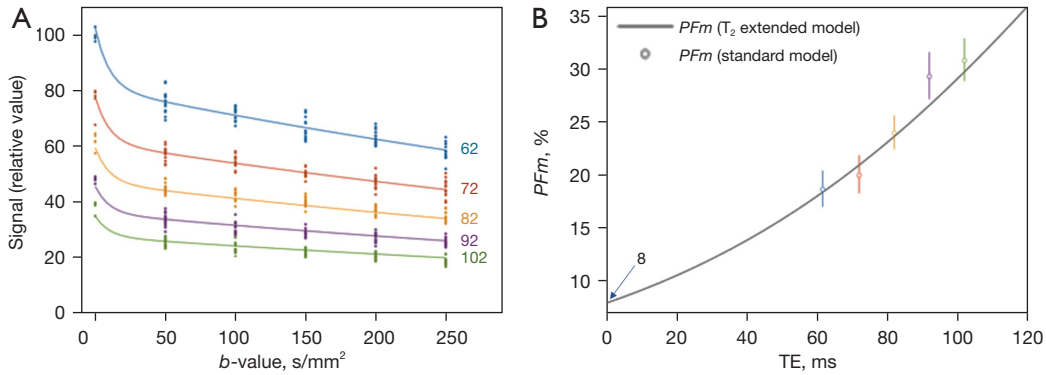

Figure 1 Five volunteer liver results from Jerome *et al.* (14). (A) Measured signal with various TE and *b*-values acquired at 1.5 Tesla. *b*-values (s/mm^2) included 0, 50, 100, 150, 200, 250; and TE (ms) included 62, 72, 82, 92, 102. Standard IVIM model was used to fit the results of each TE individually. It can be seen that the signal decay pattern following increasing *b*-values differs according to different TEs. (B) The curve is the fitting result of *PFm* with T_2 extended IVIM model. Points with 95% standard error bar represent the *PFm* values for a given TE with the standard model (color labeling is the same as in A), with a shorter TE associated with a smaller *PFm*. Note if TE =0, the curve intersects Y-axis at the value of around 8% (arrow). The figures are reproduced with permission [Jerome *et al.* (14)]. *PFm*, measured perfusion fraction; TE, time of echo; IVIM, intravoxel incoherent motion.

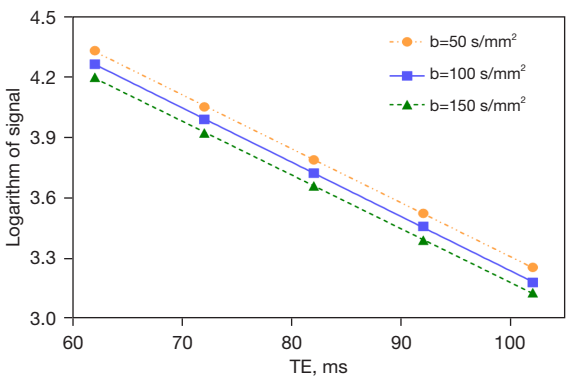

Figure 2 A high repeatability of the T_{2t} measurement is shown. Measured signal with various TE and a specific *b*-value were used to obtain T_{2t} according to Eq. [6], with the slope indicating $-1/T_{2t}$. The high level of similarity of the slopes of lines suggests a high repeatability of T_{2t} regardless of the choice of *b*-values. Data from Jerome *et al.* (14). TE, time of echo; T_{2t}, T_2 of the tissue diffusion component.

longer T_{2a}. Note that T_2 does not change much over the range of field strengths used for routine clinical MRI (0.2 to 3.0 T) (32). Considering that blood flow contribution to each tissue voxel's T_{2a} is small, T_{2a} of HCC can be assumed to be same as its T_{2t}. T_{2p} of HCC has not been measured with T_2 extended IVIM model. However, T_{2p} of HCC will be longer than liver tissue as HCC contains a larger portion of arterial blood. *Figures 3,4* show the estimated result of *PFm* based on modeling results of the study of Jerome *et al.* (14) and measured T_{2p}/T_{2t} results in literature, respectively. In *Figure 3*, the *PFm* of liver tissue is 0.157. *PFm* of HCC varies from 0.099 to 0.118 when T_{2p} changes from the value equals to liver venous blood 180 ms to the value of arterial blood 250 ms. Increase of HCC's T_{2p} will slightly mitigate the *PFm* underestimation relative to liver tissue but the underestimation caused by T_2 effect is always observable. In *Figure 4*, the same phenomenon is observed. *PFm* of liver tissue is 0.202 while *PFm* of HCC may vary from 0.138 to 0.149 depending on the T_{2p} values assumed.

In conclusion, underestimation of HCC *PFm* caused by T_2 effect due to the elongation of T_{2a} time of HCC relative to the liver is present during the standard IVIM measurement. The analysis in this letter can help to explain the much lower *PFm* observed for the spleen than for the liver (0.09 *vs.* 0.18) as spleen has a longer T_{2a} value than liver (18,33). The analysis in this letter may partially help to explain the recent observation that for tissue with T_{2a} <60 ms, a negative correlation is noted with T_{2a} time and apparent diffusion coefficient (ADC) (33). The analysis in this letter may also partially help to explain the paradoxical observation of Schmid-Tannwald *et al.* (34) that hypervascular liver metastases demonstrate significantly lower ADC values compared to hypovascular metastases, as hypervascular lesion will have a longer T_{2a} than hypovascular lesion. Liver fibrosis has been consistently shown to have a reduced *PFm* by IVIM measure even at an early

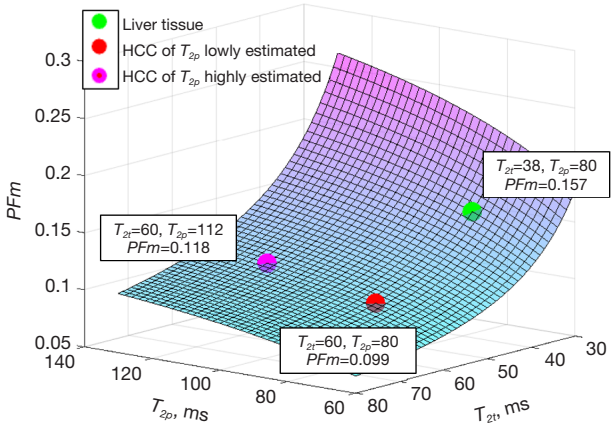

Figure 3 Change of *PFm* following the deviation of HCC T_{2t} and T_{2p} from native liver values [values based on modeling results of Jerome *et al.* (14)], showing an elongation of T_{2t} of HCC leading to an underestimation of *PFm*. The estimation of *PFm* is based on Eq. [7] with assumed *PF* =0.08 and TE =55 ms. Liver parenchyma (green ball) is assumed to have T_{2t} of 38 ms and T_{2p} of 80 ms (14), then *PFm* will be 0.157. If an HCC has T_{2t} of 60 ms (27-29) and its T_{2p} remains the same as liver, then *PFm* will decrease to 0.099 (red ball). T_{2p} of arterial blood is reported to be around 250 ms, while that of venous blood is 180 ms (22). HCC contains a much greater proportion of arterial blood (than the liver) which means HCC would have a higher T_{2p}. If HCC is mostly supplied with arterial blood, and assuming liver is mostly supplied with venous blood, thus we assume an HCC has T_{2t} and T_{2p} of 60 ms and 112 ms [i.e., considering (180/250) = (80/112)], then *PFm* will be 0.118 (pink ball). Therefore, underestimation of HCC *PFm* will always exist even if HCC T_{2p} increases dramatically relative to liver T_{2p}. More likely HCC *PFm* will be between the result of red ball and the result of pink ball. HCC, hepatocellular carcinoma; *PFm*, measured perfusion fraction; T_{2t}, T_2 of the tissue diffusion component; T_{2p}, T_2 of the perfusion component; TE, time of echo.

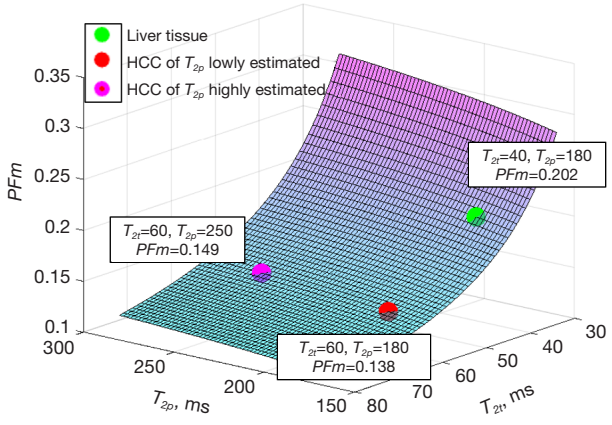

Figure 4 Change of *PFm* following the deviation of HCC T_{2t} and T_{2p} from native liver values (values based on literature), showing an elongation of T_{2t} of HCC leading to an underestimation of *PFm*. The estimation of *PFm* is based on Eq. [7] with assumed *PF* =0.08 and TE =55 ms. T_{2p} of arterial blood is reported to be around 250 ms, while that of venous blood is 180 ms (24-26). If liver T_{2p} of 180 ms is assumed to be close to that of venous blood, and liver T_{2t} is 40 ms (19-21), then *PFm* is 0.202 (green ball). If an HCC has T_{2t} of 60 ms (25-27) and its T_{2p} remains the same as liver (180 ms), then *PFm* will decrease to 0.138 (red ball). HCC contains a greater proportion of arterial blood which will measure higher T_{2p}. If HCC is mostly supplied with arterial blood, we assume an HCC has T_{2t} of 60 ms and T_{2p} of 250 ms, then *PFm* will be 0.149 (pink ball). Note that liver T_{2p} is likely to be higher than 180 ms due to its 25% arterial blood supply and HCC T_{2p} is likely to be lower than 250 ms with some extent of venous blood supply. Under these conditions, liver *PFm* will be higher and HCC *PFm* will be lower than the values indicated above, therefore the underestimation of HCC *PFm* relative to liver will be even greater. HCC, hepatocellular carcinoma; *PFm*, measured perfusion fraction; T_{2t}, T_2 of the tissue diffusion component; T_{2p}, T_2 of the perfusion component; TE, time of echo.

stage (35,36). Liver fibrosis is also noted to be associated with an increased T_{2a} (37,38). Though pathophysiologically liver fibrosis is indeed associated with perfusion reduction (39-41), the *PFm* measured by standard IVIM could also have overestimated the extent of its reduction (or it could be a false positivity for the early-stage liver fibrosis cases). In the opposite direction, we noted that a higher liver iron content, and thus the associated shortening of T_{2a}/T_2*, may be associated with a higher liver *PFm* (42). In a healthy volunteer liver DWI study, it was noted that older subjects with higher liver iron content and thus shorter T_2* and T_{2a} demonstrated higher *PFm* relative to younger subjects (43). Based on empirical observations, it has been suggested that, for standard modeling, IVIM *PFm* and D_s are 'mutually constrained' (43-45). If one parameter changes toward one direction (e.g., decreasing), then the other changes toward to the opposite direction (e.g., increasing). A reduction of *PFm* of brain tissue has been noted to be associated with an increase of D_s (45). Considering T_2 change is a major contributor to ADC change (33), and on the other hand for the standard IVIM modeling it does not appear that there is a mathematical reason that *PFm* and D_s have to be 'mutually

constrained', we may hypothesize that the 'mutually constraining' of *PFm* and D_s are moderated by T_2.

Acknowledgments

The authors thank Mr. Ben-Heng Xiao, at the Chinese University of Hong Kong, for helpful discussions during the manuscript preparation.
Funding: This work was supported by Hong Kong GRF Project (No. 14112521).

Footnote

Conflicts of Interest: Both authors have completed the ICMJE uniform disclosure form (available at https://qims.amegroups.com/article/view/10.21037/qims-23-1437/coif). Y.X.J.W. serves as the Editor-in-Chief of *Quantitative Imaging in Medicine and Surgery*. The other author has no conflicts of interest to declare.

Ethical Statement: The authors are accountable for all aspects of the work in ensuring that questions related to the accuracy or integrity of any part of the work are appropriately investigated and resolved.

References

1. Yang ZF, Poon RT. Vascular changes in hepatocellular carcinoma. Anat Rec (Hoboken) 2008;291:721-34.
2. Taskaeva I, Bgatova N. Microvasculature in hepatocellular carcinoma: An ultrastructural study. Microvasc Res 2021;133:104094.
3. Sahani DV, Holalkere NS, Mueller PR, Zhu AX. Advanced hepatocellular carcinoma: CT perfusion of liver and tumor tissue--initial experience. Radiology 2007;243:736-43.
4. Abdullah SS, Pialat JB, Wiart M, Duboeuf F, Mabrut JY, Bancel B, Rode A, Ducerf C, Baulieux J, Berthezene Y. Characterization of hepatocellular carcinoma and colorectal liver metastasis by means of perfusion MRI. J Magn Reson Imaging 2008;28:390-5.
5. Pahwa S, Liu H, Chen Y, Dastmalchian S, O'Connor G, Lu Z, Badve C, Yu A, Wright K, Chalian H, Rao S, Fu C, Vallines I, Griswold M, Seiberlich N, Zeng M, Gulani V. Quantitative perfusion imaging of neoplastic liver lesions: A multi-institution study. Sci Rep 2018;8:4990.
6. Ippolito D, Capraro C, Casiraghi A, Cestari C, Sironi S. Quantitative assessment of tumour associated neovascularisation in patients with liver cirrhosis and hepatocellular carcinoma: role of dynamic-CT perfusion imaging. Eur Radiol 2012;22:803-11.
7. Wáng YXJ. Living tissue intravoxel incoherent motion (IVIM) diffusion MR analysis without b=0 image: an example for liver fibrosis evaluation. Quant Imaging Med Surg 2019;9:127-33.
8. Xiao BH, Huang H, Wang LF, Qiu SW, Guo SW, Wáng YXJ. Diffusion MRI Derived per Area Vessel Density as a Surrogate Biomarker for Detecting Viral Hepatitis B-Induced Liver Fibrosis: A Proof-of-Concept Study. SLAS Technol 2020;25:474-83.
9. Penner AH, Sprinkart AM, Kukuk GM, Gütgemann I, Gieseke J, Schild HH, Willinek WA, Mürtz P. Intravoxel incoherent motion model-based liver lesion characterisation from three b-value diffusion-weighted MRI. Eur Radiol 2013;23:2773-83.
10. Zhu L, Cheng Q, Luo W, Bao L, Guo G. A comparative study of apparent diffusion coefficient and intravoxel incoherent motion-derived parameters for the characterization of common solid hepatic tumors. Acta Radiol 2015;56:1411-8.
11. Woo S, Lee JM, Yoon JH, Joo I, Han JK, Choi BI. Intravoxel incoherent motion diffusion-weighted MR imaging of hepatocellular carcinoma: correlation with enhancement degree and histologic grade. Radiology 2014;270:758-67.
12. Shan Y, Zeng MS, Liu K, Miao XY, Lin J, Fu Cx, Xu PJ. Comparison of Free-Breathing With Navigator-Triggered Technique in Diffusion Weighted Imaging for Evaluation of Small Hepatocellular Carcinoma: Effect on Image Quality and Intravoxel Incoherent Motion Parameters. J Comput Assist Tomogr 2015;39:709-15.
13. Hectors SJ, Wagner M, Besa C, Bane O, Dyvorne HA, Fiel MI, Zhu H, Donovan M, Taouli B. Intravoxel incoherent motion diffusion-weighted imaging of hepatocellular carcinoma: Is there a correlation with flow and perfusion metrics obtained with dynamic contrast-enhanced MRI? J Magn Reson Imaging 2016;44:856-64.

14. Jerome NP, d'Arcy JA, Feiweier T, Koh DM, Leach MO, Collins DJ, Orton MR. Extended T2-IVIM model for correction of TE dependence of pseudo-diffusion volume fraction in clinical diffusion-weighted magnetic resonance imaging. Phys Med Biol 2016;61:N667-80.
15. Lemke A, Laun FB, Simon D, Stieltjes B, Schad LR. An in vivo verification of the intravoxel incoherent motion effect in diffusion-weighted imaging of the abdomen. Magn Reson Med 2010;64:1580-5.
16. Greenway CV, Stark RD. Hepatic vascular bed. Physiol Rev 1971;51:23-65.
17. Lautt WW. Hepatic vasculature: a conceptual review. Gastroenterology 1977;73:1163-9.
18. Yu WL, Xiao BH, Ma FZ, Zheng CJ, Tang SN, Wáng YXJ. Underestimation of the spleen perfusion fraction by intravoxel incoherent motion MRI. NMR Biomed 2023;36:e4987.
19. Li YT, Cercueil JP, Yuan J, Chen W, Loffroy R, Wáng YX. Liver intravoxel incoherent motion (IVIM) magnetic resonance imaging: a comprehensive review of published data on normal values and applications for fibrosis and tumor evaluation. Quant Imaging Med Surg 2017;7:59-78.
20. Chevallier O, Wáng YXJ, Guillen K, Pellegrinelli J, Cercueil JP, Loffroy R. Evidence of Tri-Exponential Decay for Liver Intravoxel Incoherent Motion MRI: A Review of Published Results and Limitations. Diagnostics (Basel) 2021;11:379.
21. Wall SD, Fisher MR, Amparo EG, Hricak H, Higgins CB. Magnetic resonance imaging in the evaluation of abscesses. AJR Am J Roentgenol 1985;144:1217-21.
22. de Bazelaire CM, Duhamel GD, Rofsky NM, Alsop DC. MR imaging relaxation times of abdominal and pelvic tissues measured in vivo at 3.0 T: preliminary results. Radiology 2004;230:652-9.
23. Bogaert J, Claessen G, Dresselaers T, Masci PG, Belge C, Delcroix M, Symons R. Magnetic resonance relaxometry of the liver - a new imaging biomarker to assess right heart failure in pulmonary hypertension. J Heart Lung Transplant 2022;41:86-94.
24. Barth M, Moser E. Proton NMR relaxation times of human blood samples at 1.5 T and implications for functional MRI. Cell Mol Biol (Noisy-le-grand) 1997;43:783-91.
25. Stefanovic B, Pike GB. Human whole-blood relaxometry at 1.5 T: Assessment of diffusion and exchange models. Magn Reson Med 2004;52:716-23.
26. Golay X, Silvennoinen MJ, Zhou J, Clingman CS, Kauppinen RA, Pekar JJ, van Zijl PC. Measurement of tissue oxygen extraction ratios from venous blood T(2): increased precision and validation of principle. Magn Reson Med 2001;46:282-91.
27. Ohtomo K, Itai Y, Furui S, Yashiro N, Yoshikawa K, Iio M. Hepatic tumors: differentiation by transverse relaxation time (T2) of magnetic resonance imaging. Radiology 1985;155:421-3.
28. Reimer P, Weissleder R, Brady TJ, Yeager AE, Baldwin BH, Tennant BC, Wittenberg J. Experimental hepatocellular carcinoma: MR receptor imaging. Radiology 1991;180:641-5.
29. Onaya H, Itai Y, Ahmadi T, Yoshioka H, Okumura T, Akine Y, Tsuji H, Tsujii H. Recurrent hepatocellular carcinoma versus radiation-induced hepatic injury: differential diagnosis with MR imaging. Magn Reson Imaging 2001;19:41-6.
30. Olcott EW, Li KC, Wright GA, Pattarelli PP, Katz DS, Ch'en IY, Daniel BL. Differentiation of hepatic malignancies from hemangiomas and cysts by T2 relaxation times: early experience with multiply refocused four-echo imaging at 1.5 T. J Magn Reson Imaging 1999;9:81-6.
31. Goldberg MA, Hahn PF, Saini S, Cohen MS, Reimer P, Brady TJ, Mueller PR. Value of T1 and T2 relaxation times from echoplanar MR imaging in the characterization of focal hepatic lesions. AJR Am J Roentgenol 1993;160:1011-7.
32. Bottomley PA, Foster TH, Argersinger RE, Pfeifer LM. A review of normal tissue hydrogen NMR relaxation times and relaxation mechanisms from 1-100 MHz: dependence on tissue type, NMR frequency, temperature, species, excision, and age. Med Phys 1984;11:425-48.
33. Wáng YXJ, Ma FZ. A ri-phasic relationship between T2 relaxation time and magnetic resonance imaging (MRI)-derived apparent diffusion coefficient (ADC). Quant Imaging Med Surg 2023. doi: 10.21037/qims-23-1342.
34. Schmid-Tannwald C, Thomas S, Ivancevic MK, Dahi F, Rist C, Sethi I, Oto A. Diffusion-weighted MRI of metastatic liver lesions: is there a difference between hypervascular and hypovascular metastases? Acta Radiol 2014;55:515-23.
35. Wáng YXJ, Wang X, Wu P, Wang Y, Chen W, Chen H, Li J. Topics on quantitative liver magnetic resonance imaging. Quant Imaging Med Surg 2019;9:1840-90.
36. Li T, Che-Nordin N, Wáng YXJ, Rong PF, Qiu SW, Zhang SW, Zhang P, Jiang YF, Chevallier O, Zhao F, Xiao XY, Wang W. Intravoxel incoherent motion derived liver perfusion/diffusion readouts can be reliable biomarker

for the detection of viral hepatitis B induced liver fibrosis. Quant Imaging Med Surg 2019;9:371-85.
37. Guimaraes AR, Siqueira L, Uppal R, Alford J, Fuchs BC, Yamada S, Tanabe K, Chung RT, Lauwers G, Chew ML, Boland GW, Sahani DV, Vangel M, Hahn PF, Caravan P. T2 relaxation time is related to liver fibrosis severity. Quant Imaging Med Surg 2016;6:103-14.
38. Takayama Y, Nishie A, Ishimatsu K, Ushijima Y, Fujita N, Kubo Y, Yoshizumi T, Kouhashi KI, Maehara J, Akamine Y, Ishigami K. Diagnostic potential of T1ρ and T2 relaxations in assessing the severity of liver fibrosis and necro-inflammation. Magn Reson Imaging 2022;87:104-12.
39. Van Beers BE, Leconte I, Materne R, Smith AM, Jamart J, Horsmans Y. Hepatic perfusion parameters in chronic liver disease: dynamic CT measurements correlated with disease severity. AJR Am J Roentgenol 2001;176:667-73.
40. Wagner WL, Föhst S, Hock J, Kim YO, Popov Y, Schuppan D, Schladitz K, Redenbach C, Ackermann M. 3D analysis of microvasculature in murine liver fibrosis models using synchrotron radiation-based microtomography. Angiogenesis 2021;24:57-65.
41. Zhang W, Huang C, Yin T, Miao X, Deng H, Zheng R, Ren J, Chen S. Ultrasensitive US Microvessel Imaging of Hepatic Microcirculation in the Cirrhotic Rat Liver. Radiology 2023;307:e220739.
42. Xiao BH, Wáng YXJ. Different tissue types display different signal intensities on b = 0 images and the implications of this for intravoxel incoherent motion analysis: Examples from liver MRI. NMR Biomed 2021;34:e4522.
43. Huang H, Zheng CJ, Wang LF, Che-Nordin N, Wáng YXJ. Age and gender dependence of liver diffusion parameters and the possibility that intravoxel incoherent motion modeling of the perfusion component is constrained by the diffusion component. NMR Biomed 2021;34:e4449.
44. Wáng YXJ. Mutual constraining of slow component and fast component measures: some observations in liver IVIM imaging. Quant Imaging Med Surg 2021;11:2879-87.
45. Wáng YXJ. A reduction of perfusion can lead to an artificial elevation of slow diffusion measure: examples in acute brain ischemia MRI intravoxel incoherent motion studies. Ann Transl Med 2021;9:895.

Cite this article as: Ma FZ, Wáng YXJ. T_2 relaxation time elongation of hepatocellular carcinoma relative to native liver tissue leads to an underestimation of perfusion fraction measured by standard intravoxel incoherent motion magnetic resonance imaging. Quant Imaging Med Surg 2024;14(1):1316-1322. doi: 10.21037/qims-23-1437

